J Mol Model (2002) 8:87–94
DOI 10.1007/s00894-002-0077-x

ORIGINAL PAPER

**Timothy Clark · Bernd Bleisteiner · Siegfried Schneider**

# Excited state conformational dynamics of semiflexibly bridged electron donor-acceptor systems: a semiempirical CI-study including solvent effects

Received: 27 November 2001 / Accepted: 10 February 2002 / Published online: 21 March 2002


**Abstract** Semiempirical (AM1) molecular orbital theory with configuration interaction has been used to investigate the harpooning mechanism proposed from experimental studies on semiflexibly bridged electron donor-acceptor systems. Our calculations on the charge-transfer state of N-phenyl-4-(4-cyano-naphth-1-ylmethyl)-piperidine, **1**, confirm the proposed harpooning mechanism including an intermediate loosely folded charge-transfer state and reproduce the thermodynamics obtained from our spectroscopic studies closely. The structural details of the extended (ECT), intermediate (ICT) and compact (CCT) charge-transfer states are discussed, as are the transition states connecting them. Solvent effects have been modeled using self-consistent reaction field (SCRF) calculations within the polarized continuum model. The effect of solvent polarity on the stabilities of the three charge-transfer states is discussed.

**Keywords** Semiempirical MO-theory · AM1 · Excited states · Charge transfer · Solvation

## Introduction

Experimental studies on semiflexibly bridged electron donor-acceptor systems [1, 2, 3, 4, 5, 6, 7, 8, 9, 10] have revealed many important details about the dynamics of the long lived charge-transfer (CT) states and have given rise to a detailed mechanistic proposal not only of the structures involved for the CT states, but also of their relative stabilities in solution. [10] Briefly, the experimental results were interpreted as indicating that for derivatives of N-phenyl-4-(4-cyano-naphth-1-ylmethyl)-piperidine, **1**, an initial extended CT-state (ECT), **2**, first converts to an intermediate, loosely folded (ICT) structure, **3**, before collapsing to the final compact (CCT) structure **4** (see Scheme 1). The experimental studies have provided such a detailed picture of the conformational dynamics of the system that we have now performed semiempirical (AM1) [11] molecular orbital configuration interaction (CI) calculations on the charge-transfer states of **1** both in order to obtain more microscopic details of the reaction mechanism than are available from experiment and to test the applicability of the calculation techniques for such a relatively complicated excited state system with simulated solvent effects.

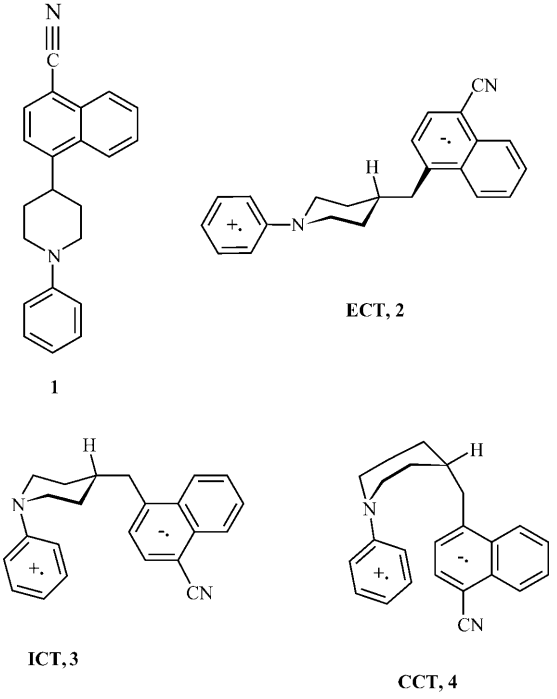


**Scheme 1** Structures of the compounds investigated with their abbreviations

T. Clark (✉)
Computer-Chemie-Centrum der Universität Erlangen-Nürnberg,
Nägelsbachstraße 25, 91054 Erlangen, Germany
e-mail: Clark@chemie.uni-erlangen.de

B. Bleisteiner · S. Schneider
Institut für Physikalische und Theoretische Chemie
der Universität Erlangen-Nürnberg,
Egerlandstraße 3, 91058 Erlangen, Germany

## Methods

All calculations were performed with VAMP 7.5 [12] using the standard AM1 Hamiltonian. [11] Geometry optimizations with configuration interaction (CI) used analytical gradients [13] along with a CI expansion using all singly excited states and the doubly excited states in which an intact electron pair is promoted [14] between the two highest occupied and the two lowest virtual orbitals (PECI=4). Test CI calculations with very much larger active orbital windows showed that this level is adequate for the problem in hand. Transition states were optimized using either Baker's Eigenvector-Following (EF) technique [15] or Powell's NS01A. [16] Minima and transition states were confirmed as such by calculating the normal vibrations using second derivatives evaluated numerically from the analytical first derivatives. However, this was not possible with our current software for ICT, **3**, for which the finite step differentiation procedure enters the region of a conical intersection (see below) and for the conical intersection ("TS2", **6**) itself. All geometry optimizations were performed *in vacuo*. Ground state geometry optimizations for minima used the restricted Hartree-Fock (RHF) formalism and were started from the optimized geometry of the charge-transfer state in the corresponding conformation. The interconversion transition states for the ground state were calculated using the methods described above with the RHF-formalism. The calculated gas phase heats of formation for the optimized structures are shown in Table 1.

Calculations of spectra used a CI-expansion involving all single excitations within 24 active orbitals (12 occupied and 12 virtual, CIS=24). Self-consistent reaction field (SCRF) [17] calculations used our published technique [18] with natural atomic orbital/point charge (NAO-PC) [19] electrostatics and included non-equilibrium solvation for absorption/fluorescence spectra. [20] The dispersion correction presented in our original treatment was not included in the SCRF-treatment. The SCRF-calculations used the geometries obtained from the *in vacuo* optimizations. The cavities used were based on the solvent-excluded surface [21] determined by a modification of the Marsili marching cube algorithm [22] with GEPOL. [23] Van der Waals radii taken from Bondi [24] were increased by 20% in order to calculate the cavities.

**Table 1** Optimized heats of formation (kcal $mol^{-1}$) for the ground (AM1-HF) and charge-transfer (AM1, PECI=4) states calculated *in vacuo*. The data shown in parentheses for **2** and **5** are for the second, less stable conformation in which the naphthalene group is rotated by roughly 180° compared to the conformation discussed throughout. The spectral properties of this conformation are very similar to those for the more stable rotamer

| Species | Ground state[a] | Charge-transfer state |
|---|---|---|
| ECT, **2** | 92.23 (92.78) | 210.05 (211.07) |
| TS1, **5** | 95.87 (95.79) | 212.11 (212.14) |
| ICT, **3** | 93.04 | 200.93 |
| "TS2", **6** | 99.45 | 201.53 |
| CCT, **4** | 96.25 | 190.75 |

[a] Geometry obtained by optimization starting from the optimized geometry of the corresponding conformation of the charge-transfer state and therefore expected to be the minimum on the ground state potential energy surface that is given by geometrical relaxation of the Franck-Condon state reached by a vertical transition from the CT to the ground state.

## Structures and electronic properties of the charge-transfer conformations

### The extended charge-transfer (ECT) structure

The AM1/CI optimized structure of the ECT, 2, is shown in Fig. 1. The central piperidine ring adopts a chair conformation with the donor and acceptor groups in equatorial positions as expected. The cyanonaphthalene acceptor occupies a position staggered 60° relative to the axial hydrogen at the 4-position of the piperidine. There are thus two sets of diastereomeric ECT enantiomers. The structure shown as 2 is the more stable (by 1.0 kcal $mol^{-1}$) and will be used for further discussion. The total charges calculated by summing the Coulson atomic charges of the fragments obtained by dissecting the molecule at the naphthyl-$CH_2$-bond are $\pm 1.06$ $e^-$, indicating complete charge separation. The calculated dipole moment is 35.5 Debye (35.7 in hexane solution). The distance between the positive and negative charge centers is approximately 6.6 Å.

### The intermediate charge-transfer (ICT) structure

Figure 2 shows the optimized structure obtained for the intermediate charge-transfer (ICT) structure, **3**. The piperidine ring in this conformation still adopts a chair conformation, but the N-phenyl group now occupies the axial position and the naphthalene acceptor is rotated by approximately 120° about the piperidine-$CH_2$-bond to a position *transoid* to the axial hydrogen at $C_4$ of the piperidine ring. These changes bring the donor

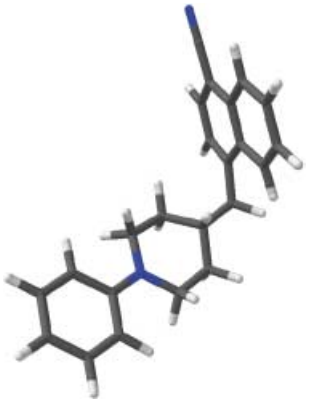

**Fig. 1** The AMI (PECI=4) optimized geometry of the ECT-conformation **2**


**Fig. 2** The AMI (PECI=4) optimized geometry of the ICT-conformation **3**


**Fig. 3** The AMI (PECI=4) optimized geometry of the CCT-conformation **4**

and acceptor aromatic rings into an essentially parallel alignment with inter-ring distances between 4.5 and 5 Å, as shown by the representative distances marked in Figure 2. The total charges, calculated as above, for the donor and acceptor units are ±0.65 $e^-$ and the calculated dipole moment is 12.8 Debye. The charge separation is thus calculated to be incomplete and the dipole moment is smaller than that observed experimentally. [10] The relatively small charge separation calculated for this species in the gas phase, however, results from strong mixing with a non-polar locally excited state. This mixing is removed in solution, giving complete charge separation and a dipole moment of 21.5 Debye (see below).

### The compact charge-transfer (CCT) structure

Figure 3 shows the optimized geometry of the CCT-structure, **4**. The piperidine ring adopts a twisted boat conformation with both the donor and the acceptor substituents axial. The inter-ring distance is significantly shorter than in the ICT structure, **3**, between 3.4 and 4 Å. The charge separation is calculated to be ±1.04 $e^-$ and the dipole moment 16.8 Debye (17.0 in hexane). Thus, the charge-transfer in the CCT is complete despite the close approach of the two aromatic systems. It might be expected that the close approach of the donor and acceptor aromatic rings might lead to some back-donation, but this is not found.

**Fig. 4** The AMI (PECI=4) optimized geometry of the transition state for conversion of ECT, **2**, into ICT, **3**

## Interconversion transition states

### ECT to ICT

The conversion of ECT, **2**, to ICT, **3**, simply involves a 120° rotation about the piperidine-$CH_2$-bond. The transition state **5** is later than the purely eclipsed conformation, with a CCCC-dihedral angle of 21.6°. The naphthalene system is perpendicular to the mean piperidine plane so that the aromatic ring can rotate past the ring methylene protons with the minimum of steric repulsion. The N-phenyl system is planar with a total of the three bond angles at nitrogen of 359.7°. The calculated dipole moment (36.7 Debye) is the largest found for the conformations of the charge-transfer state investigated. The optimized geometry is shown in Fig. 4.

### ICT to CCT

The conversion from **3** to **4** is not as simple as the bond rotation needed to convert **2** into **3**. In the gas phase, the charge-transfer state in the CCT-conformation is strongly stabilized so that it lies lower in energy than the lowest locally excited state. As, however, this locally excited state is $S^1$ for ICT, **3**, the conversion from **3** to **4** involves at best an avoided crossing between these two states. We believe, however, that a conical intersection lies between these two structures with approximately the geometry **6** shown in Fig. 5. The calculated gas phase energy difference between the two lowest lying excited singlet states at this geometry is 0.002 eV and the energy gradients become discontinuous at or near this geometry. This, of course, means that interconversion process will be considerably different in solution to that in the gas phase. However, as analytical CI gradients are not yet available within the SCRF model, we have used geometry **6** to calculate the "activation energy" for the folding process to CCT in solution.

Structure **6**, however, has roughly the geometry expected for an early transition state for the exothermic rearrangement of **3** to **4**. The piperidine ring is slightly flattened at the $C_4$-end compared to **3** and the naphthalene

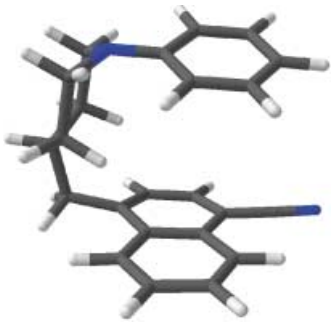

**Fig. 5** The AMI (PECI=4) geometry of the structure **6** that we believe to be very close to a conical intersection connecting the ICT-conformation **3** with the CCT-conformation, **4**

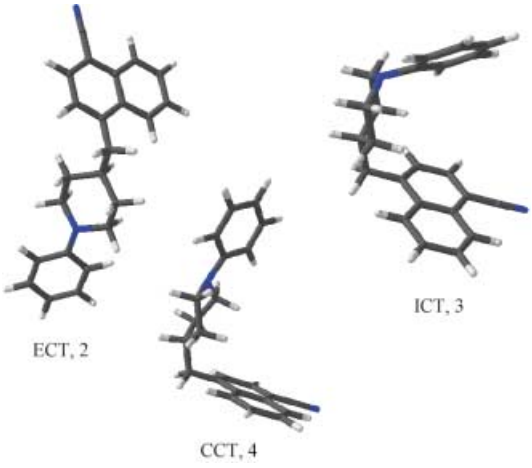


**Fig. 6** Ground state geometries obtained by optimization starting from the corresponding charge-transfer state structures

acceptor has begun to swing through into the axial position in a twist boat conformation of the central ring. The N-$C_4$-distance in the piperidine is increased from 2.92 Å in **3** to 3.03 Å in **5**, although the ring still adopts a flattened chair conformation.

## Gas phase energies

As expected for the gas phase, the folding of the ECT to give first ICT and then CCT, both of which are stabilized by significant Coulomb attraction between the donor$^{+\cdot}$ and the acceptor$^{-\cdot}$ moieties, is an exothermic process. A crude calculation suggests that, if we decrease the distance between a positive and a negative charge from the 6.6 Å donor-acceptor distance estimated above for **2** to the 5.5 Å inter-ring distance calculated for **3,** the Coulomb stabilization should increase by 10 kcal mol$^{-1}$ and decreasing the distance to 4.5 Å should provide a further 13 kcal mol$^{-1}$ stabilization. In fact, ICT, **3**, is calculated to be 9 kcal mol$^{-1}$ more stable than ECT, **2**, and CCT, **4**, a further 10 kcal mol$^{-1}$ more stable than ICT, **3**, suggesting that the simple electrostatic picture can capture the main features of the gas phase thermodynamics of this system. Axial-equatorial and chair-twist boat energy differences would correct the crude electrostatic estimate in the right direction. Note, however, that we did not find complete charge-separation for ICT, **3**. The factors affecting the electronic nature and stability of this structure will be discussed in more detail below.

The activation energy for the conversion from **2** to **3**, a simple rotation about the piperidine-$CH_2$-bond, is calculated to be 2.1 kcal mol$^{-1}$. This value is likely to be low because of the known tendency of semiempirical techniques to underestimate barriers to rotation about single bonds. [25] Nevertheless, the barrier for a 120° rotation to give a product that is 10 kcal mol$^{-1}$ more stable should not be very much higher than our calculations suggest, even for this relatively crowded system.

Structure **6**, which we believe to be close to the conical intersection connecting ICT, **3**, with CCT, **4**, in the gas phase, lies 1.1 kcal mol$^{-1}$ higher in energy than **3**. The proximity of this conical intersection to **3** makes numerically evaluated second derivatives for **3** unreliable, so that we were unable to confirm **3** as a local minimum with our current software. However, as we have been able to find the transition state connecting **2** and **3**, we are confident that **3** is indeed a local minimum.

## Ground state geometries

The ground state geometries corresponding to **2-4** were optimized using the structures of charge-transfer state conformations as starting points. We performed these calculations in order to be able to rule out that direct excitation of a stable ground state conformation could give either ICT, **3** or CCT, **4**. The calculated heats of formation (Table 1) suggest that only the ground state ECT, **2**, need be considered. The structures obtained are shown in Fig. 6.

The ECT-structure **2** relaxes 8.7 kcal mol$^{-1}$ to give a very similar structure to that found in the charge-transfer state. The ICT-structure **3** retains both the ring conformation and the axial position of the phenyl ring to give a structure that is relaxed 8.5 kcal mol$^{-1}$ compared to that of the charge-transfer state and is only 0.8 kcal mol$^{-1}$ higher in energy than the ground state ECT-structure. The bond-rotation transition state connecting these two structures (not shown in Fig. 6) lies 3.6 kcal mol$^{-1}$ higher in energy than the ground state ECT-structure. The CCT-conformation **4** undergoes considerable (13.9 kcal mol$^{-1}$) geometrical relaxation to give a twist boat conformation with the phenyl group in an equatorial position, as shown in Fig. 6. This structure is 4 kcal mol$^{-1}$ less stable than the ground state ECT-structure and the barrier for the ring inversion from the ground state ICT-conformation is 6.4 kcal mol$^{-1}$.

## SCRF calculations

Initially, SCRF single point energy calculations were performed using the physical properties of *n*-hexane for

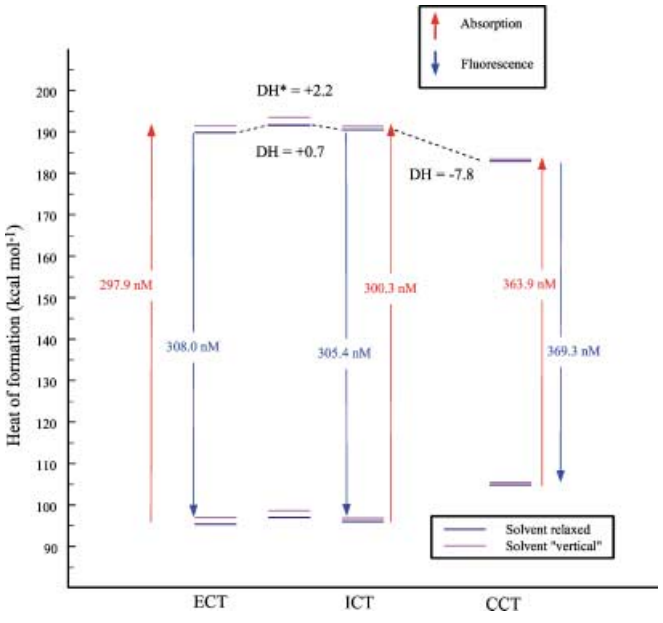


**Fig. 7** Schematic energy level diagram for the three charge-transfer structures, **2**–**4**, and the "transition states" (**5** and **6**) connecting them. The heats of formation are calculated at the optimized gas phase structures of the excited states using the PECI=4 CI-expansion with which the geometries were optimized. The energies of the same states calculated at the ground-state geometries are also shown

the solvent continuum in order to be able to compare our calculations directly with the experimental data, [10] which were obtained in methylcyclohexane solution. The results are shown in Fig. 7 and show remarkable agreement with the thermodynamic details deduced from the experimental results. The rotation about the piperidine-$CH_2$-bond in **2** to give **3** *via* transition state **5** proceeds with a low activation energy (2.2 kcal $mol^{-1}$) and is found to be enthalpically slightly endothermic, in excellent agreement with the experimental results. The change from the gas phase reaction, which is about 9 kcal $mol^{-1}$ exothermic, to solution is not caused primarily by a change in dipole moment on folding, but rather by a decrease in the surface area of the molecule available for solvation. The aromatic donor and acceptor moieties can only be solvated fully on their outer faces in the ICT, **3**, so that this species is roughly 10 kcal $mol^{-1}$ less well solvated than the easily accessible ECT **2**. The difference between the two folded conformations **3** and **4** is less pronounced, so that the final folding process is calculated to be enthalpically favorable by almost 8 kcal $mol^{-1}$, again in remarkable agreement with experiment.

The electronic properties of ICT, **3**, change quite dramatically between the gas phase and hexane solution. This is because **3** lies close to the crossing between the lowest CT- and local excitation (LE) singlets in the gas phase and the calculated wavefunction therefore contains significant contributions from the two states. This makes the CT-state less polar and the LE-state more so. The result is that, as outlined above, the charge separation in the gas phase is only about 65% complete. In the SCRF-calculations the CT-state is stabilized preferentially and therefore moved in energy away from the LE-state. The mixing found in the gas phase therefore becomes insignificant and the observed charge-separation in ICT, **3**, is ±1.0185 and the calculated dipole moment 21.5 Debye. Fig. 8 shows plots of the first four singlet energy levels found in the PECI=4 calculations along the reaction coordinate. In the gas phase the CT-state crosses both locally excited states between ICT, **3**, and CCT, **4**. The gas phase plot clearly shows the interaction between the CT-state and the higher locally excited one (labelled LE2). In hexane solution, the CT-state must only cross the lowest locally excited singlet and this crossing occurs well after "TS2", **6**.

## Discussion

### ECT gas phase spectrum

Table 2 shows the calculated gas phase spectrum of the ground state structure corresponding to ECT, **2**. The

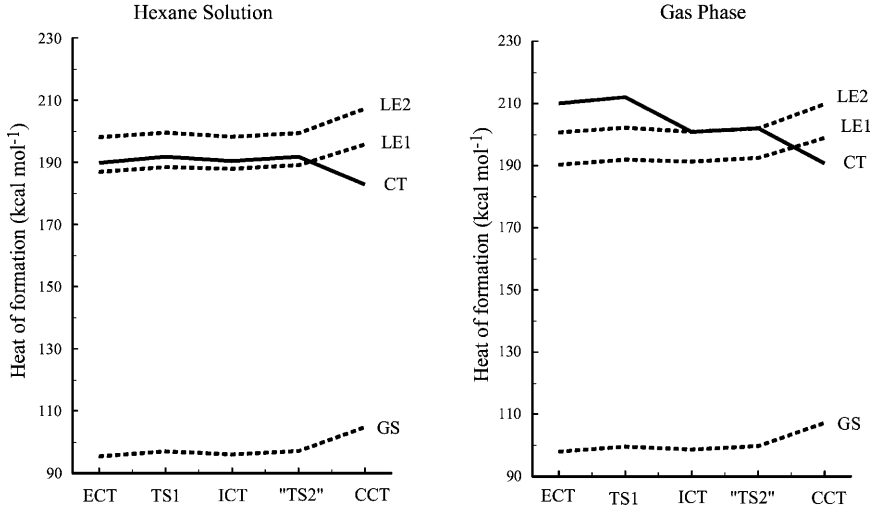


**Fig. 8** The energy levels of the four lowest singlet states obtained in the PECI=4 calculations as a function of the reaction coordinate. The crossings are shown as if they were not weakly avoided (the system has no symmetry)

**Table 2** Calculated relative energies, excitation wavelengths and oscillator strengths for the singlet states of ECT, **2** *in vacuo*. The calculations were performed at the optimized geometry of the ground state using a singles CI with 24 active orbitals

| State | Heat of formation (kcal mol$^{-1}$) | Energy relative to $S^0$ (eV) | Dipole Moment (Debye) | $\lambda_{vertical}$ (nm) | Oscillator strength | Assignment[a] |
|---|---|---|---|---|---|---|
| $S^0$ | 92.2 | 0.0 | 2.94 | – | – | Ground state |
| $S^1$ | 173.2 | 3.51 | 3.11 | 353.0 | 0.013 | LE (naphthalene) |
| $S^2$ | 174.8 | 3.58 | 3.54 | 346.4 | 0.135 | LE (naphthalene) |
| $S^3$ | 179.1 | 3.77 | 2.59 | 329.2 | 0.010 | LE (aniline) |
| $S^4$ | 182.3 | 3.91 | 2.86 | 317.4 | 0.095 | LE (aniline) |
| $S^5$ | 195.0 | 4.45 | 3.86 | 278.3 | 0.006 | Amino $n\rightarrow\sigma^*$ |
| $S^6$ | 198.8 | 4.62 | 3.47 | 268.4 | 0.063 | LE (naphthalene) |
| $S^7$ | 204.1 | 4.85 | 4.11 | 255.6 | 0.065 | LE (naphthalene) |
| $S^8$ | 212.4 | 5.21 | 4.25 | 237.9 | 0.349 | LE (aniline) |
| $S^9$ | 215.0 | 5.32 | 2.86 | 232.9 | 1.314 | LE (naphthalene) |
| $S^{10}$ | 217.9 | 5.45 | 9.42 | 227.5 | 0.261 | LE (naphthalene) |
| $S^{11}$ | 222.4 | 5.65 | 5.44 | 219.6 | 0.453 | LE (naphthalene) |
| $S^{12}$ | 223.1 | 5.67 | 11.14 | 218.6 | 0.358 | LE (naphthalene) |
| $S^{13}$ | 224.1 | 5.72 | 29.09 | 216.8 | 0.091 | CT (HOMO → LUMO) |
| $S^{14}$ | 233.0 | 6.11 | 15.62 | 203.1 | 0.001 | CT (naphthalene → cyano) |

[a] LE = local excitation; CT = charge-transfer

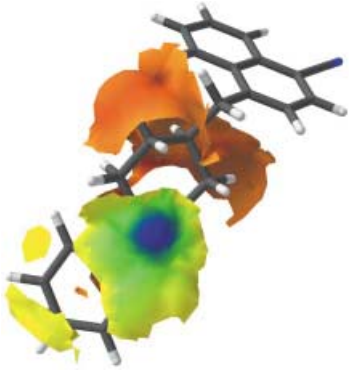

**Fig. 9** Change in molecular electrostatic potential (the energy of interaction of a unit positive charge) at the surface of ECT on excitation from $S^0$ to $S^5$ (gas phase state-ordering). Only the areas of the surface for which the MEP changes by more than 5 kcal mol$^{-1}$ are shown. *Red* represents a higher electron density (and hence potential) in the excited state and *blue* the reverse

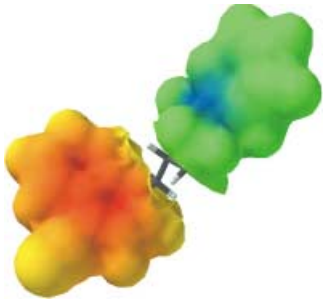

**Fig. 10** Change in molecular electrostatic potential (the energy of interaction of a unit positive charge) at the surface of ECT on excitation from $S^0$ to $S^{13}$ (gas phase state-ordering). Only the areas of the surface for which the MEP changes by more than 20 kcal mol$^{-1}$ are shown. *Red* represents a higher electron density (and hence potential) in the excited state and *blue* the reverse

"$\lambda_{vertical}$" values reported in the table are the vertical transition wavelengths at the Born-Oppenheimer geometry of the ground state. The calculated spectrum holds few surprises. The lowest energy singlet states are formed by local excitations within the naphthalene moiety, followed by corresponding LE states for the aniline-group. $S^5$ is the first state with some CT-character. However, this state does not show long-range charge separation between the aniline donor and the naphthalene acceptor, but is rather a local $n\rightarrow\sigma^*$ excitation at the aniline amino-group. This excitation results in some charge transfer from the nitrogen lone-pair to the piperidine-ring, as shown in Fig. 9, which shows the change in the molecular electrostatic potential (MEP) at the surface of the molecule on excitation.

$S^6$ to $S^{12}$ are LE-states, mostly in the naphthalene chromophore. $S^{13}$, however, is the CT-state produced by a HOMO to LUMO excitation and involves the transfer of one electron from the aniline moiety to the cyanonaphthalene, as shown by the MEP-difference plot given in Fig. 10. The sharpness of the boundary between the donor and acceptor parts of the molecule is quite remarkable.

The final singlet state shown in Table 2, $S^{14}$, also involves a charge-transfer element, but in this case from the naphthalene to the cyano-group. Figure 11 shows the change in the surface MEP on excitation from the ground state to $S^{14}$.

## ECT spectrum in hexane-solution

Table 3 shows the effect of the simulated hexane solvent on the calculated spectrum of ECT. The heats of formation are calculated with a fully relaxed solvent for the excited state, whereas the vertical excitation energies refer to the "slow" solvent polarization component from the ground state. [18, 20] The energetic ordering of the lowest seven singlet states remains the same as that found for the gas phase, but the donor-acceptor charge-

**Table 3** Calculated relative energies, vertical excitation wavelengths and oscillator strengths for ECT, **2** , in a simulated hexane solvent. The calculations were performed at the optimized geometry of the ground state using a singles CI with 24 active orbitals. Data for the excited states correspond to ground-state solvation with electronic polarization [19, 20] and may therefore differ slightly from the data given in the text for fully relaxed solvation of the excited states.

| State | Equivalent in vacuo | Heat of formation (kcal mol$^{-1}$, relaxed solvent) | Energy relative to $S^0$ (eV) | Dipole Moment (Debye) | λ vertical (nm) ("vertical solvent") | Oscillator strength | Assignment[a] |
|---|---|---|---|---|---|---|---|
| $S^0$ | $S^0$ | 89.4 | 0.0 | 3.42 | – | – | Ground state |
| $S^1$ | $S^1$ | 170.4 | 3.51 | 3.65 | 353.3 | 0.016 | LE (naphthalene) |
| $S^2$ | $S^2$ | 171.7 | 3.57 | 4.11 | 347.4 | 0.134 | LE (naphthalene) |
| $S^3$ | $S^3$ | 176.2 | 3.76 | 3.01 | 329.6 | 0.010 | LE (aniline) |
| $S^4$ | $S^4$ | 179.2 | 3.89 | 3.20 | 318.6 | 0.095 | LE (aniline) |
| $S^5$ | $S^5$ | 193.5 | 4.51 | 4.24 | 274.8 | 0.006 | Amino $n\rightarrow\sigma^*$ |
| $S^6$ | $S^6$ | 195.6 | 4.60 | 4.13 | 269.4 | 0.065 | LE (naphthalene) |
| $S^7$ | $S^7$ | 200.7 | 4.82 | 4.81 | 257.0 | 0.082 | LE (naphthalene) |
| $S^8$ | $S^{13}$ | 206.9 | 5.09 | 32.84 | 241.1 | 0.050 | CT (HOMO → LUMO) |
| $S^9$ | $S^8$ | 207.7 | 5.13 | 4.43 | 241.6 | 0.336 | LE (aniline) |
| $S^{10}$ | $S^{10}$ | 210.6 | 5.26 | 9.76 | 235.5 | 0.247 | LE (naphthalene) |
| $S^{11}$ | $S^9$ | 212.0 | 5.31 | 3.39 | 233.3 | 1.263 | LE (naphthalene) |
| $S^{12}$ | $S^{14}$ | 212.7 | 5.35 | 16.51 | 230.6 | 0.000 | CT (naphthalene → cyano) |
| $S^{13}$ | $S^{11}$ | 217.1 | 5.54 | 5.61 | 223.6 | 0.452 | LE (naphthalene) |
| $S^{14}$ | $S^{12}$ | 219.5 | 5.64 | 8.68 | 219.7 | 0.429 | LE (naphthalene) |

[a] LE = local excitation; CT = charge-transfer

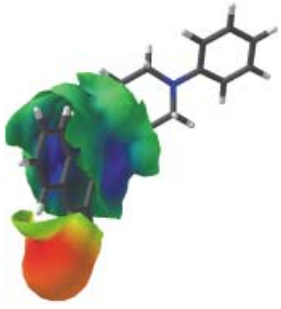

**Fig. 11** Change in molecular electrostatic potential (the energy of interaction of a unit positive charge) at the surface of ECT on excitation from $S^0$ to $S^{14}$ (gas phase state-ordering). Only the areas of the surface for which the MEP changes by more than 20 kcal mol$^{-1}$ are shown. *Red* represents a higher electron density (and hence potential) in the excited state and *blue* the reverse

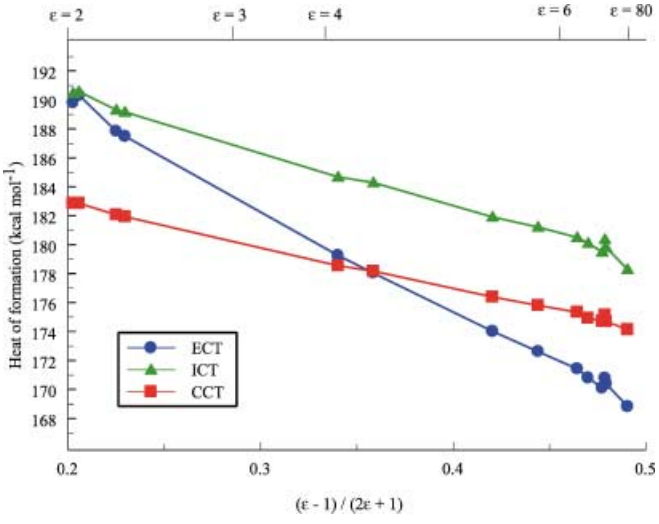


**Fig. 12** Calculated heats of formation of the three charge-transfer conformations as a function of solvent polarity

transfer state ($S^{13}$ in the gas phase) is now found to be $S^8$. The most intense LE-absorption (to $S^9$ in the gas phase, to $S^{11}$ in solution) is found at a shorter wavelength in solution than that for the transition to CT-state. The naphthalene to cyano CT-state ($S^{15}$ in the gas phase) is also stabilized in solution and becomes $S^{12}$.

## Solvent effects

Figure 12 shows the results of SCRF calculations on the three minima (ECT, ICT and CCT) with a total of 14 solvents ranging from hexane to water and plotted against the solvent polarity factor (ε–1)/(2ε+1), where ε is the macroscopic dielectric constant.

The initial ECT-state is most strongly stabilized by increasingly polar solvents, so that it becomes the most stable of the three conformations at a solvent polarity corresponding roughly to ether. The folded CCT-state is less strongly stabilized by polar solvents for two reasons; it has a dipole moment about half as large as that found for ECT and one face each of the aromatic donor and acceptor are not accessible to the solvent. Similarly, the intermediate ICT, with the smallest calculated dipole moment of the three conformations, is only weakly stabilized by polar solvents. Fig. 11 thus suggests not only that CCT should become energetically less favorable relative to ECT in more polar solvents, but also that it should become kinetically less easily accessible because the intermediate ICT-state becomes too high in energy in polar

solvents, in accordance with the experimental observation that harpooning is only observed in solvents with $\varepsilon \leq 4$.

Interestingly, the experiments indicate that the isomerization from ECT, **2**, to ICT, **3**, involves a slight increase in enthalpy, as calculated here, but a decrease in the free energy. We are unable to calculate the free energy for this process because of the problems outlined above calculating the normal vibrations of **3**. However, as an indication, the zero-point vibrational energy of CCT, **4**, which ought to be similar to that of ICT, **3**, is 0.7 kcal $mol^{-1}$ higher than that of ECT, **2**. Thus, the zero-point energy, vibrational and entropic corrections should favor **3** over **2**, as found experimentally.

## Conclusions

Our calculations allow us to draw two important conclusions; firstly, the interpretation of the excited state conformational dynamics of the subject systems derived from the spectroscopic studies is confirmed in remarkable detail and, secondly, semiempirical CI-calculations with a SCRF-simulation of the solvent are very successful in reproducing the behavior of this system. Especially the relative energies and the low activation barriers for interconversion of ECT, ICT and CCT are reproduced extremely well by the calculations. The calculated spectra show some systematic deviations, but the trends are also well reproduced. Our current inability to optimize excited states within an SCRF-model does not appear to affect the quality of the results seriously. However, for a process such as the conversion of ICT to CCT, which we believe to occur *via* a conical intersection, solvent effects shift the intersecting states significantly and thus may change the results.

**Acknowledgments** This work was supported by the Deutsche Forschungsgemeinschaft via the Graduiertenkolleg *"Homogener und heterogener Elektronentransfer"*, the Volkswagen Foundation and the Fonds der Chemischen Industrie.

## References

1. Borkent JH, De Jong AW, Verhoeven JW, de Boer T J (1978) Chem Phys Lett 57:530–534
2. Wegewijs B, Hermant RM, Verhoeven JW, De Haas MP, Warman JM (1990) Chem Phys Lett 168:185–190
3. Verhoeven JW, Scherer T, Willemse RJ (1993) Puer Appl Chem 65:1717–1722
4. van Stokkum IHM, Scherer T, Brouwer AM, Verhoeven JW (1994) J Phys Chem 98:852–866
5. van Stokkum IHM, Scherer T, Brouwer AM, Verhoeven JW (1994) J Phys Chem 98:10539–10549
6. Verhoeven JW, Wegewijs B, Scherer T, Rettschnik RPH, Warman JM, Jäger W, Schneider S (1996) J Phys Org Chem 9:387–397
7. Wegewijs B, Ng AKF, Verhoeven JW (1995) Recl Trav Chim Pays-Bas 114:6–12
8. Jäger W, Schneider S, Lauteslager XY, Verhoeven JW (1996) J Phys Chem 100:8118–8124
9. Lauteslager XY, van Stokkum IHM, van Ramesdonk HJ, Brouwer AM, Verhoeven JW (1999) J Phys Chem 103:653–659
10. Bleisteiner B, Marian T, Schneider S, Brouwer AM, Verhoeven JW (2001) Phys Chem Chem Phys 3:2070–2079
11. (a) Dewar MJS, Zoebisch EG, Healy EF, Stewart JJP (1985) J Am Chem Soc 107:3902–3909, (b) Holder AJ (1998) In: Schleyer PVR, Allinger NL, Clark T, Gasteiger J, Kollman PA, Schaefer III HF, Schreiner PR (eds) Encyclopedia of Computational Chemistry, vol.1. Wiley, Chichester, p 8
12. Clark T, Alex TA, Beck B, Chandrasekhar J, Gedeck P, Horn A, Hutter M, Martin B, Rauhut G, Sauer W, Schindler T, Steinke T (2000) Vamp 7.5. Oxford Molecular, The Medawar Center, Oxford Science Park, Sandford–on–Thames, Oxford OX4 4GA, United Kingdom.
13. Dewar MJS, Liotard DA (1990) J Mol Struct (Theochem) 206:123–133
14. Clark T, Chandrasekhar J (1994) Israel J Chem 33:435–448
15. Baker J (1986) J Comput Chem 7:385–395
16. Powell MJD (1982) Non-linear Optimizations. Academic Press, New York
17. Tomasi J, Mennucci B (1998) In: Schleyer PVR, Allinger NL, Clark T, Gasteiger J, Kollman PA, Schaefer III HF, Schreiner PR (eds) Encyclopedia of Computational Chemistry, vol. 4. Wiley, Chichester, p 2547
18. Rauhut G, Clark T, Steinke T (1993) J Am Chem Soc 115:9174–9181
19. (a) Rauhut G, Clark T (1993) J Comput Chem 14:503–509, (b) Beck B, Rauhut G, Clark T (1994) J Comput Chem 15:1064–1073
20. Gedeck P, Schneider S (1997) J Photochem Photobiol A: Chemistry 105:165–182
21. Pascual-Ahuir JL, Silla E, Tuñon I (1994) J Comput Chem 15:1127–1138
22. (a) Marsili M, Floersheim P, Dreiding AS (1983) Comp Chem 7:175–181, (b) Lorensen W, Cline H (1987) Comp Graph 21:163
23. Pascual-Ahuir JL, Silla E, Tomasi J, Bonnaccorsi R (1988) GEPOL, Quantum Chemistry Program Exchange, Program Nr. 554, University of Indiana
24. Bondi A (1964) J Phys Chem 68:441–451
25. Clark T (1985) A Handbook of Computational Chemistry. Wiley-Interscience, New York